Journal of Hydrosciences and Environment
ISSN: 2345-5608

Hydrodynamic characteristics of lock-exchange flow in curve channels in the presence of blocks

E. Hamzenejad[1], Gh. Azizyan[2,*], B. Pirzadeh[3], A. Abdollahi

1. Master student, Civil Engineering Department, University of Sistan and Baluchestan, Zahedan, Iran.
2,. Associate Professor, Civil Engineering Department, University of Sistan and Baluchestan, Zahedan, Iran*
3. Associate Professor, Civil Engineering Department, University of Sistan and Baluchestan, Zahedan, Iran.
4. Ph.D., Civil Engineering Department, University of Sistan and Baluchestan, Zahedan, Iran

ARTICLEINFO

Article history:

Received: 29 Jan 2020
Accepted: 10 Oct 2020

Keywords:
OpenFOAM
Curved Channel
Gravity Current Block
Lock
Exchange.

ABSTRACT

Gravity current is the flow of fluid through another fluid of varying density. This flow often occurs in nature. For optimal management of water resource quality, it is necessary to know and study the gravity current. Naturally, many streams have a meandering path. There are also many blocks in different shapes (both natural and artificial). Therefore, in the present study, to control a lock-exchange gravity current, a triangular, rectangular, or trapezoidal rigid barrier was placed inside a curved channel with a curvature of 120 degrees and a radius (R) of one meter. Simulations were performed using the OpenFoam open-source software and the realizable k-ε turbulence model. The Reynolds number was 19700 in all of them. According to previous studies, in a block-free channel, the most secondary current occurs in the middle of the curve. In this study, to control the secondary current, the blocks were placed at 60 degrees of the curve. With an impediment, the secondary current was visible in the body and tail of the current but did not occur in the current head. The obstacle affected the pattern of the secondary currents so that the pattern was different around the block from the other locations. The barrier also reduced the spanwise velocity of the flow body. The concentration was maximum at the head of the stream, indicating that the barrier could affect the concentration along the stream so that the maximum concentration was behind the block. The current head was also affected by the block, as it did not advance for a moment on the inner bank; at these moments, the outer bank surpassed the inner bank.

1. Introduction

Gravity current or density current is the flow by which a high-density fluid diffuses horizontally into a low-density fluid along the bottom of a channel. Cold, or hot currents, polluted currents, winds, etc., are among the gravity currents that occur naturally in lakes, oceans, and atmospheres (Ungarish, 2009). The driving force, caused by the density difference, is between two fluids, which can be due to the difference in their temperature or density or because of suspended particles. Gravity current has three phases. The current head diffuses in the first phase at a constant velocity. The second phase can be an inert phase where the velocity and depth of the current are reduced. The third phase occurs if the Reynolds number of the gravity current is sufficiently reduced (Huppert et al., 1980; Hacker et al., 1996).

The lock-exchange method means that two fluids of different densities are initially stationary by a vertical gate. Immediately, after the gate removal, the heavier (denser) fluid moves horizontally and below the less dense fluid due to the difference in hydrostatic pressure along the bottom of the tank. In comparison, the lighter fluid moves in the opposite direction and along the upper boundary of the reservoir (Simpson, 1997; Shin et al., 2004).

Gravity current typically carries hazards. So far, gravity-current studies have been performed in various fields. To identify and minimize these hazards, researchers have investigated various areas of lock-exchange gravity current, including the movement of gravity current on a sloping and horizontal surface, the effect of the presence of rigid and permeable blocks with different shapes on the flow path, and the flow inside a curved channel. This article refers to some of these cases. Some of these studies on horizontal beds have been performed in a laboratory and some have used numerical simulations. Examples include Lombardi et al. (2018), Ottolenghi et al. (2016), Yin et al. (2020), and Ottolenghi et al. (2020). In addition, Lombardi et al. (2015), He et al. (2018), Ottolenghi et al. (2016), de Falco et al. (2020), and Steenhauer et al. (2017) have examined gravity current on slopes. Kneller and Buckee (2000) focused their study on the structure and behavior of gravity currents containing particles, such as submarine currents.

In addition to laboratory studies, numerical simulations can also be used. Several researchers have studied gravity

*Corresponding author's email: g.azizyan@eng.usb.ac.ir

DOR: 20.1001.1.23455608.2020.4.8.4.5

current using Navier-Stokes numerical models. LES, DNS, and RANS are high-resolution models that provide a complete description of gravity currents. Ooi et al., (2009), Tokyay et al. (2011), and Ottolenghi et al. (2016) have used LES, Özgökmen et al. (2004), Chang et al. (2005), Härtel et al. (2000), and Cantero et al. (2006) have used DNS, and Paik et al. (2009), Huang et al. (2005), and Sequeiros (2012) have used RANS in their studies.

Hacker et al. (1996) studied the gravity current in straight channel lock-exchange topics, high Reynolds number (19700), and a 12% density difference between the two fluids for the first time in the laboratory. Many researchers, including Mahdinia et al. (2012), Ooi et al. (2009), and Paik et al. (2009), have employed Hacker et al.'s second experiment (1996) as the basis for their research.

According to Magdaleno and Fernández-Yuste (2011), most rivers naturally flow in a symmetrical meandering path. When there are meanders in the flow path, the flow structure becomes complex in the channel's length, width, and depth (Ikeda & McEwan, 2009). The secondary currents have a spiral structure in the meanderings channel. The end of each form is the beginning of another. Extensive research has been done on the identification and study of secondary current in the straight and meandering flow path (Wormleaton et al., 1982; Knight & Demetriou, 1983; Knight & Hamed, 1984).

Mahdinia et al. (2012) conducted his lock-exchange studies numerically at a 90-degree curve of a channel without the presence of an impediment. The results showed that the characteristics of the current in the body position of the current were similar to the submarine gravity current in that the secondary current occurred near the bottom of the channel and in the longitudinal position of its apex while no secondary current was observed in the head position of the current. On the other hand, the secondary current pattern was different in the tail position.

Installing a block on the current bed in front of a diffusing gravity current can cause many changes in the flow structure. This is true both for currents whose density difference is related to temperature and salinity and for currents in which the presence of particles causes a density difference. If the height of the installed block is sufficient for the current's height, it can act as a flow controller and change the flow regime (Rottman et al., 1985; Lane-Serff et al., 1995). Impediments in the flow can stop or weaken the flow. They can also direct the gravity currents away from structures affected by sediments. On the other hand, these blocks can divert the flow to areas where dredging is less (Tokyay & Constantinescu, 2015). Ozan et al. (2015), Tokyay et al. (2011), Wu and Ouyang (2020), Huang et al. (2020), and Zhou and Venayagamoorthy (2017, 2020) investigated the effect of an impediment on the gravity current dynamics.

Blocks may naturally exist on a curved path. The presence of a block within curved channels can cause new phenomena. Since the effect of the presence of a block in the curve has not been studied in gravity current discussions so far, the present paper investigates this phenomenon in a 120-degree curve, using Hacker et al.'s (1996) second experiment as the basis for research.

2. Materials and Methods

2.1. Numerical methods

In the present study, OpenFOAM software was used for simulation. OpenFOAM is a Computational Fluid Dynamics (CFD) toolbox that can model problems related to single-phase and multiphase currents, turbulent and laminar, heat transfer, chemical reaction, electromagnetism, solid mechanics, etc. (Abdollahi et al., 2017).

Problems with incompressible two-phase flows can be solved with the help of twoLiquidMixingFoam, a multiphase solver. This solver is based on the Volume of Fluid (VOF) method. Gauss linear divSchemes were used for the nut variable and Gauss SuperBee divSchemes were used for alpha, u, k, and epsilon. Also, among the pressure-velocity coupling algorithms, the PIMPLE algorithm (a hybrid between SIMPLE and PISO algorithms) was chosen to solve this problem. The geometry dimensions of the present study are consistent with the geometry dimensions of Mahdinia et al.'s (2012) study, except that the curve angle was 120 degrees. The maximum Courant number for all simulations did not exceed 0.3, and the value of Δt varied along the solution path. For optimal validation of concentration lines in numerical studies, it is better to use the no-slip boundary condition for walls, according to Ooi et al. (2007). Since all boundaries were walls, the boundary conditions for pressure, velocity, and turbulence fields (ν_t, k, and ε) were fixedFluxPressure, noSlip, and (nutkWallFunction, kqRWallFunction, and epsilonWallFunction), respectively. The relationships for k and epsilon are expressed at the moment zero:

$$k_0 = 3/2(UI)^2 \quad (1)$$

in which I and U are the intensity of turbulence and current head velocity, respectively.

$$\varepsilon_0 = \frac{C_\mu^{\frac{3}{4}} k_0^{\frac{3}{2}}}{l_t} \quad (2)$$

Assuming C_μ= 0.09 as the model's constant and l_t = 1/2 × height of the lock.

2.2. Governing equations and turbulence modeling

Using the VOF method, the continuity and momentum equations were solved in the present problem, which used the Boussinesq hypothesis to solve the Reynolds stress ($-\rho\overline{u'_i u'_j}$) (Ismail, 2017):

$$\frac{\partial \bar{u}_j}{\partial x_j} = 0 \quad (3)$$

$$\frac{\partial \rho \bar{u}_i}{\partial t} + \frac{\partial \rho \bar{u}_i \bar{u}_j}{\partial x_j} = -\frac{\partial \bar{p}}{\partial x_i} + \frac{\partial}{\partial x_j}\left(\mu \frac{\partial \bar{u}_i}{\partial x_j} - \rho \overline{u'_i u'_j}\right) - \rho g \delta_{ij} \quad (4)$$

$$-\rho \overline{u'_i u'_j} = \vartheta_t \left(\frac{\partial \bar{u}_i}{\partial x_j} + \frac{\partial \bar{u}_j}{\partial x_i}\right) - \frac{2}{3}\rho g \delta_{ij} \quad (5)$$

$\bar{u}_i$ equals the Reynolds average velocity in x-direction, $\bar{P}$ is the Reynolds average pressure, and g is the gravity acceleration. Moreover; in Equation (5), ϑ_t stands for the turbulence viscosity calculated by Equation 6 where k is the turbulent kinetic energy and ε is the turbulent energy dissipation rate (Ahmed et al., 2018).

$$\vartheta_t = C_\mu \rho \frac{k^2}{\varepsilon} \quad (6)$$

The selected turbulence model is realizable k – ε. In this turbulence model compared to other RANS models, the turbulence viscosity is improved by calculating the energy dissipation using more variables. In addition, it does not consider C□, which is the coefficient of the turbulence model, to be constant in Equation 6.

2.3. Problem setup

In this section, the general shape of the geometry evaluated in this research and the laboratory channel of Hacker et al. (1996) is presented (Figures 1a,b). The geometry configured is such that a curve with an angle of 120 degrees and a radius of 1 meter is located in the middle of two straight rectangular channels with lengths $x_2 = x_3 = 400$mm. In the middle of this curve, which is 120 degrees symmetrical (60 degrees), obstacles in different shapes are located perpendicular to the stream. The dimensions of the lock at the moment zero are equal to the dimensions of the second case of Hacker et al.'s (1996) study. Also, channel depth (h) and channel width (b) in all simulations are constant and equal to h = 400 mm and b = 200 mm. The vertex of the coordinate axis is at the end of the lock, where the most central transverse point of the channel is located. So, the x-axis is in the direction of the channel length, the y-axis is in the direction of height, and the z-axis is in the direction of width and towards the inner bank of the channel.

The Reynolds number and Froude number were calculated using the relations $Re = \frac{u_f h}{2\nu}$ and $Fr = u_f/u_b$. They equaled 19700 and 0.45 in the second experiment, respectively) Hacker et al., 1996).

In these relations, u_f equals the velocity of the current head, h the height of the lock, ν is the viscosity of the dense fluid, and $u_b = \sqrt{g'h}$ is the buoyancy velocity at the moment zero. Moreover; $g' = g(\rho_{max} - \rho_{min}/\rho_{min})$ is the reduced gravitational acceleration, where g is the gravitational acceleration and ρ_{max} and ρ_{min} are the density of the fluid inside the lock and the density of the surrounding fluid (ambient fluid), respectively (Hacker et al., 1996).

Mahdinia et al. (2012) investigated a channel with a 90-degree curve. According to their results, they stated that the secondary current had the highest value in the position of 45 degrees of the curve. By moving towards the head or tail of the current, the secondary current decreased. On the other hand, in the stream path of many natural rivers, there are obstacles with different shapes and geometries, natural or artificial, and these obstacles can affect the structure of the flow. Hence, to control the secondary current in the position of 60 degrees of the curve, simulations were performed in the presence of three rectangular, triangular and trapezoidal obstacles (Figure 2). The length, width, and height of all three barriers were the same. On the other hand, the width of the obstacle was equal to the width of the main channel. The height of the barrier was chosen according to Tokyay and Constantinescu (2015) to be equal to 0.3 h. The simulations performed included Hacker et al.'s (1996) laboratory model (H), curve channel without obstacle (B), curve channel with a rectangular barrier (BOR), curve channel with a triangular obstacle (BOT), and channel with trapezium barrier (BOTR).

The geometric parameters are given in Table 1, and t / t0 is when the flow head reaches the end of the channel.

Table 1. The physical parameters of the simulations.

Simulation	X_1/h	X_2/X_1	X_3/X_1	X_{o1}/X_1	X_{o2}/X_1	b/h	b_o/h	h_o/h	t/t_0	Courant maximum
H	1	-	-	-	-	0.512	-	-	6.8	0.5
B	-	1	1	-	-	0.512	-	-	14.2	0.3
BOR	-	1	1	0.1	0.1	0.512	0.512	0.3	16.9	0.3
BOT	-	1	1	0.1	-	0.512	0.512	0.3	16.7	0.3
BOTR	-	1	1	0.1	0.05	0.512	0.512	0.3	16.5	0.3

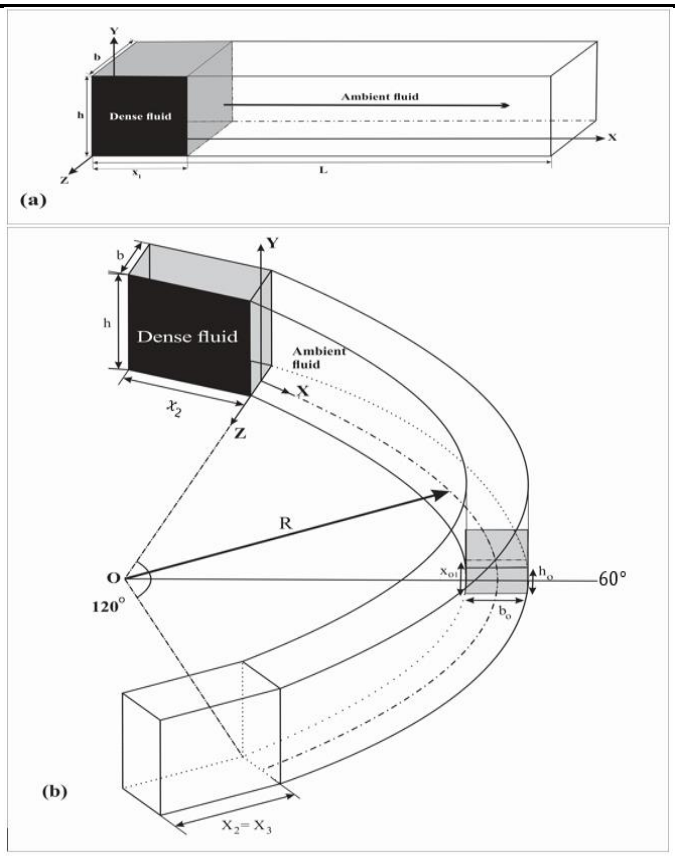


Fig. 1. A schematic of the studied geometries: a) simple channel geometry used in the validation) Hacker et al., 1996), b) channel geometry evaluated in this research.

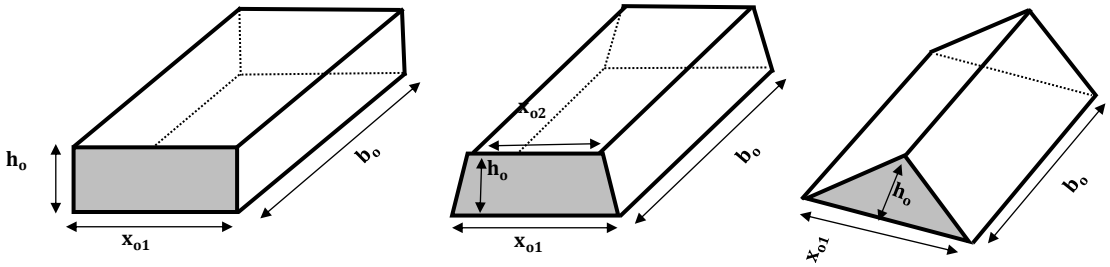


Fig. 2. The geometry of the obstacles used in the channel.

2.4. Solver validation

The second model of Hacker et al. laboratory (1996) was used to validate the numerical results. Figure (1a) shows the schematic of the channel geometry. The model was run with three mesh sizes of 1, 2, and 3 million grid to determine the mesh quality for the validation model. With the help of the blockMesh program, the organized meshes were produced. The channel floor had a boundary layer mesh. The results related to the position of the current head versus time and the mixing of the vortices were compared with the laboratory models of Hacker and Mahdinia.

According to these results, cases with 1 and 2 million cells performed slightly weaker than those with 3 million cells in terms of vortex mixing. Hence, the case with 3 million mesh serves as a validation criterion with the Hacker

laboratory model. While the time step of the solution fluctuated, the maximum Courant number during the solution was constant and equal to 0.5. It should be noted that the boundary conditions and the selected turbulence model were similar to the channel with curved features.

Figure 3 shows Hacker et al.'s (1996) simulation and experimental concentration contours. It can be seen that in the first moments after removing the lock, there are differences between the experimental results of the Hacker and the present simulation. In Hacker's experimental study, the lower and head layers of the current are ahead of the upper layers and the body of the current. In contrast, in the present simulation, the head and body of the current are symmetrical.

This discrepancy is reflected in the results of research by other researchers, including Härtel et al. (2000), Ooi et al. (2007), and Mahdinia et al. (2012). Researchers like Ooi et al. (2007, 2009) and Paik et al. (2009) have also used Hacker et al.'s (1996) second model to validate their research, stating that by applying wall boundary conditions to all boundaries, Hacker's numerical and laboratory results are more similar. On the other hand, according to the latest results and statements presented by Ooi et al., (2007), this asymmetry is due to the error of removing the laboratory gate.

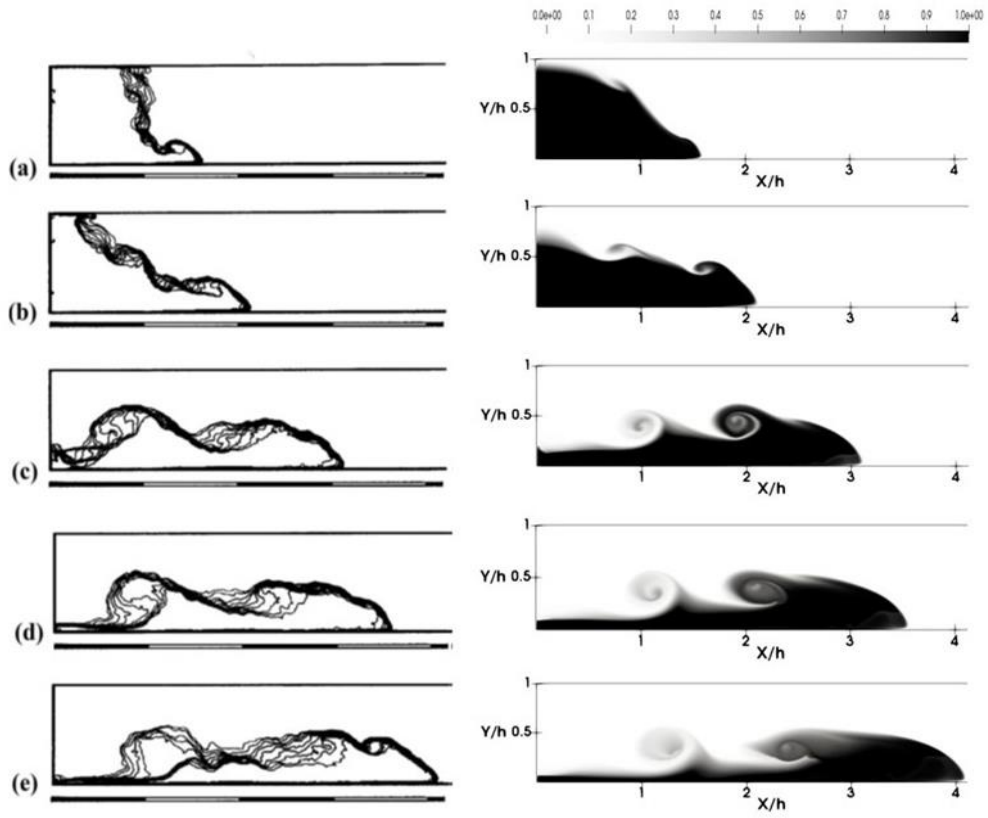


Fig. 3. The left column is Hacker's measurements from (a) to (e) and the right column are the simulations in the moments of (a) $\frac{t}{t_0} = 1.4$, (b) $\frac{t}{t_0} = 2.4$, (c) $\frac{t}{t_0} = 4.36$, (d) $\frac{t}{t_0} = 6$, and (e) $\frac{t}{t_0} = 6.26$

In Figure (4), the head position time was compared for three of the present studies and Mahdinia et al.'s (2012) and Hacker et al.'s (1996) laboratory model in which the acceptable agreement between the results of the current work and Hacker et al.'s (1996) and Mahdinia et al.'s (2012) laboratory models are evident.

2.5. Mesh sensitivity

Sensitivity analysis is an important task in many fields of engineering. In particular, advanced sensitivity techniques have gained attention among hydraulic engineers recently (Amini et al., 2021; Hariri-Ardebili et al., 2021).

The delicate sensitivity and complexity of meshing indicate the presence of an obstacle in the curve and the high Reynolds number. In this section, the mesh grids of the simulated cases, i.e., B, BOR, BOT, and BOTR, were studied.

Using snappyHexMesh and blockMesh, the solution mesh grids were classified into cubic and pyramidal meshes. Using blockMesh, a fully organized cube-based mesh was generated. Also, by using snappyHexMesh and the boundary layer mesh settings, the ultimate computing grid was created. The size and number of the meshes were different for each of the simulations as given in Table (2).

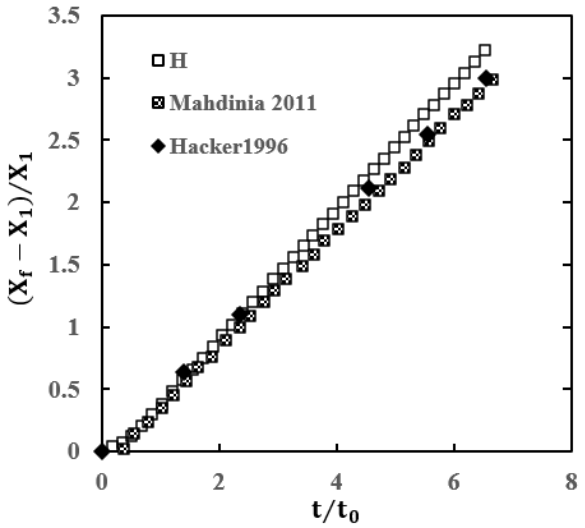


Fig. 4. Validation of the front position versus time in a straight channel without an obstacle.

Table 2. The volume of the simulation mesh.

Simulation	Number of cells in mesh (millions)		
	Run 1	Run 2	Run 3
B	1.43	3.36	4.22
BOR	1.42	3	3.89
BOTR	1.43	3.02	3.8
BOT	1.43	3.01	3.81

The parameters of spanwise velocity, front position versus time, and flow concentration were used to select the optimal mesh for calculations. This section presents observations related to spanwise velocity (Figure 6) and concentration contours (Figure 5). In general, the largest difference in the results of concentration contours (Figure 5) was observed in the position of the current head. In Figure 5, the results are very close, and there is no major difference between all three computational grids. In Figure 6, the current head in all models and the meshes' volume have reached the end of the channel. These results are for the 90-degree position around the vertical axis of the point z = 0 of the channel. As can be seen, the results are very close, and as the mesh volume increases, the difference in results decreases. Finally, the maximum number of cells in each model is a good choice for the final mesh.

According to Figures 5 and 6 and the observations not presented here, the position of the current head was not significantly different over time for three different mesh volumes. Concentration contours showed that the dense structure at the head of the flow was slightly different. Besides, at more significant mesh volumes, more detail of concentration was visible. Finally, the mesh with the most cells was selected as the final mesh in each model.

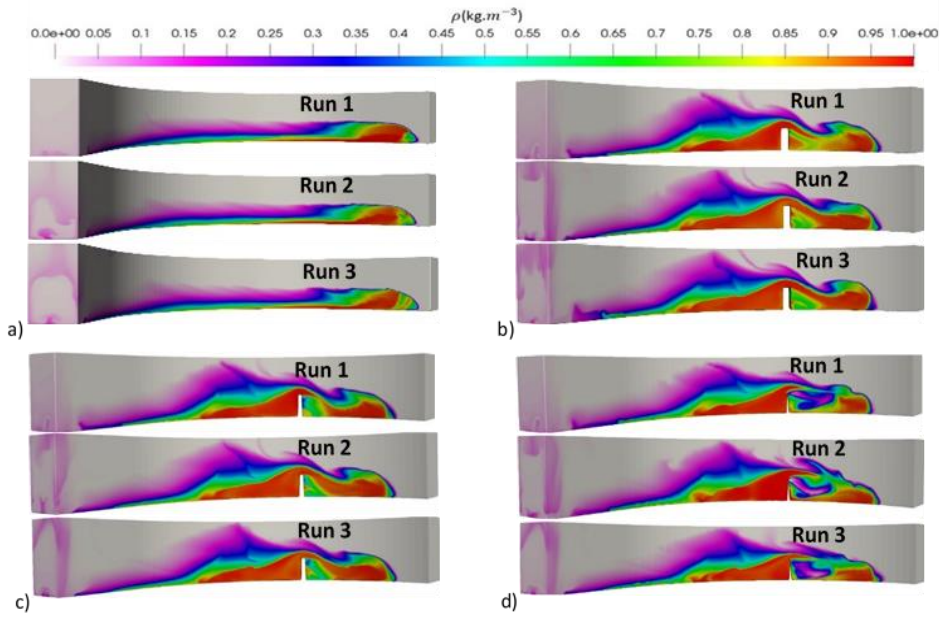


Fig. 5. Concentration contour of the interior bank view: (a) Model B – the position of the current head near the end of the channel and in $\frac{t}{t_0} = 13.7$ and (b), (c), and (d) are BOR, BOTR, and BOT cases, respectively, in which the current head is in the 90-degree position and $\frac{t}{t_0} = 11.15$.

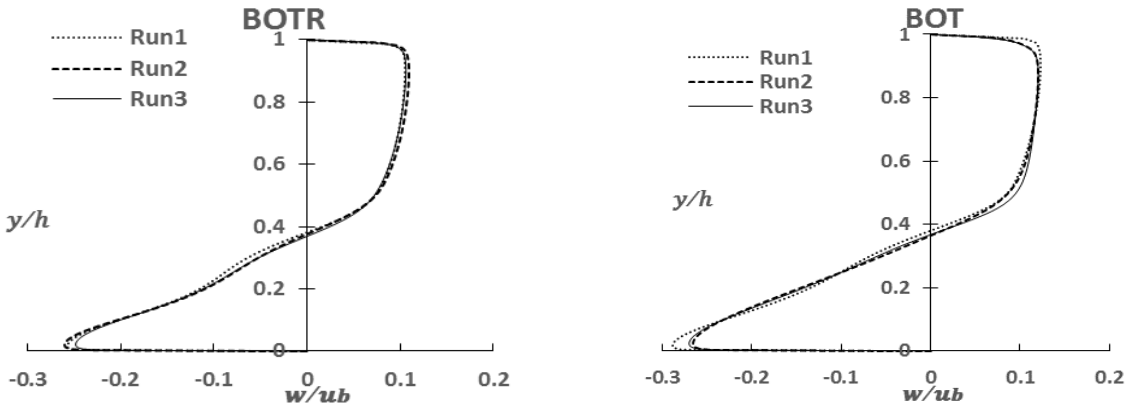


Fig. 6. Comparison of spanwise velocity data around the vertical axis at Z = 0 for three simulation mesh volumes.

3. Results and Discussion

This section reviews the results related to the position of the current head for the BOR model. The following subsections discuss flow concentration, secondary current, and streamwise velocity for BOR, BOTR, and BOT models. Then, the effect of obstacle deformation is compared by comparing all three models.

3.1. Current front position

The location of the main point of the current head relative to the initial position of the lock is defined as the position of the current front. If this point is located at the curve of a curved channel, the position of the current head is defined as r□ where r is the curve radius and □ is the angle of the channel positions. Figure (4) shows the head position versus time for a straight channel without a curve in which the slope of the line is constant, meaning that the flow evolves at a uniform speed along the channel. Figure (7) shows the front position versus time for the BOR model.

In curved channels, at the end of the simulation, the current evolves toward the inertial phase. As mentioned, in this phase, the flow velocity begins to decrease due to the channel's curve, which causes more loss and mixing of the

current. This phenomenon reduces the slope of the curved channel line compared to the straight channel (Mahdinia et al., 2012). The present study shows that an obstacle disrupts the regular and increasing trend slightly. The obstacle decreases the head velocity of the current. So, the slope of the BOR model curve versus B reduces. It is evident that a part of the curve has a zero-slope due to the

presence of the barrier. After passing the obstacle and over time, the chart's slope returns to the state before the obstacle. In the BOT and BOTR models, the curve slope changes follow the same process as BOR.

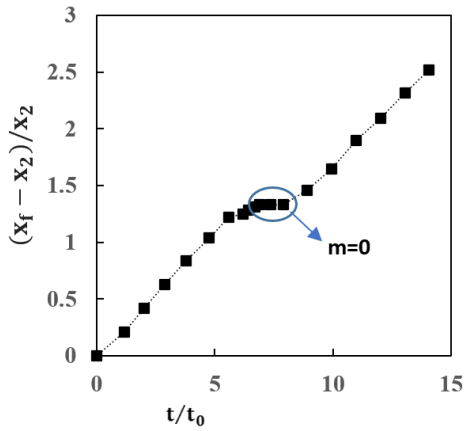


Fig. 7. The position of the front position versus time in the BOR model.

3.2. Density

According to the results of Model B, in general, the concentration at the head of the current has the highest value. It decreases towards the tail of the stream, which is evenly distributed on the cross-section of the channel. This mechanism has also been stated by Mahdinia et al. (2012). Now in the presence of the obstacle, this process is a little different and the highest concentration is observed behind the barrier. Concentration contours for other parts of the curve are given in Figure (8) for the three models of BOR, BOTR, and BOT. The 58, 61, 70, and 80-degree of the channel are the positions of the current's head, the current's body, the body immediately after the obstacle, and the body before the obstacle, respectively. In these three models, the highest concentration was observed before the obstacle. According to Figure (8), the presence of the barrier caused the lock fluid to oscillate and create discontinuities and the dense structure to be divided into two parts between the inner bank and the outer bank. Because the current velocity is high in the head position and the centrifugal force in the curve directs the lock fluid to the outer bank, at 80-degrees, the height of the dense structure on the external bank increased compared to the inner bank. These results conform with the results of 90-degree curve studies by Mahdinia et al. (2012). On the other hand, reducing the width of the upper part of the obstacle reduces the amount of concentration in the positions of the current body. It increases this amount in the position of the current head. Also, in the current head position of the BOT model, the height of the dense structure is reduced.

3.3. Secondary current

Figure 9 depicts the secondary current patterns for the studied models, including (a) BOR, (b) BOTR, and (c) BOT in the pre-obstacle positions (50 and 58°) and the post-obstacle positions (70 and 80°).

There is no secondary current in the current head, and most of the secondary current is in the body and tail. According to the given patterns, the direction of the secondary flow at the current head is from the inner bank to the external bank near the bed. It is from the outer bank to the internal bank near the interface. Also, towards the tail of the stream, the spanwise velocity distribution due to the secondary current is irregular. In the upper parts of the channel, where the fluid is clear, the amount of spanwise velocity is low. These results are consistent with Mahdinia et al. (2012) who stated that the amount of spanwise velocity in the body of the current is much higher than its head. In this study, the amount of spanwise velocity in the body of the stream decreased to a level lower than the amount of the current head in the presence of the obstacle in the channel. Also, the value of spanwise velocity decreases both before and after the obstacle, especially in the flow body. As with the concentration section, the head height of the current on the outer bank of the BOT model is lower than that of the BOR and BOTR models.

3.4. Streamwise velocity

Figure (10) shows the streamwise velocity profiles for the three studied models of (a) BOR, (b) BOTR, and (c) BOT. For each case, two pre-obstacle positions (35 and 50°) and two post-obstacle positions (61 and 80°) are shown.

According to the patterns observed in Figure (10), at the beginning of the channel and in the positions before the obstacle, the value of streamwise velocity on the inner bank is maximum, and this value is maximized on the outer bank by passing through the curve. These results are also observed in the simulation of the obstacle-free curve channel by Mahdinia et al. (2012).

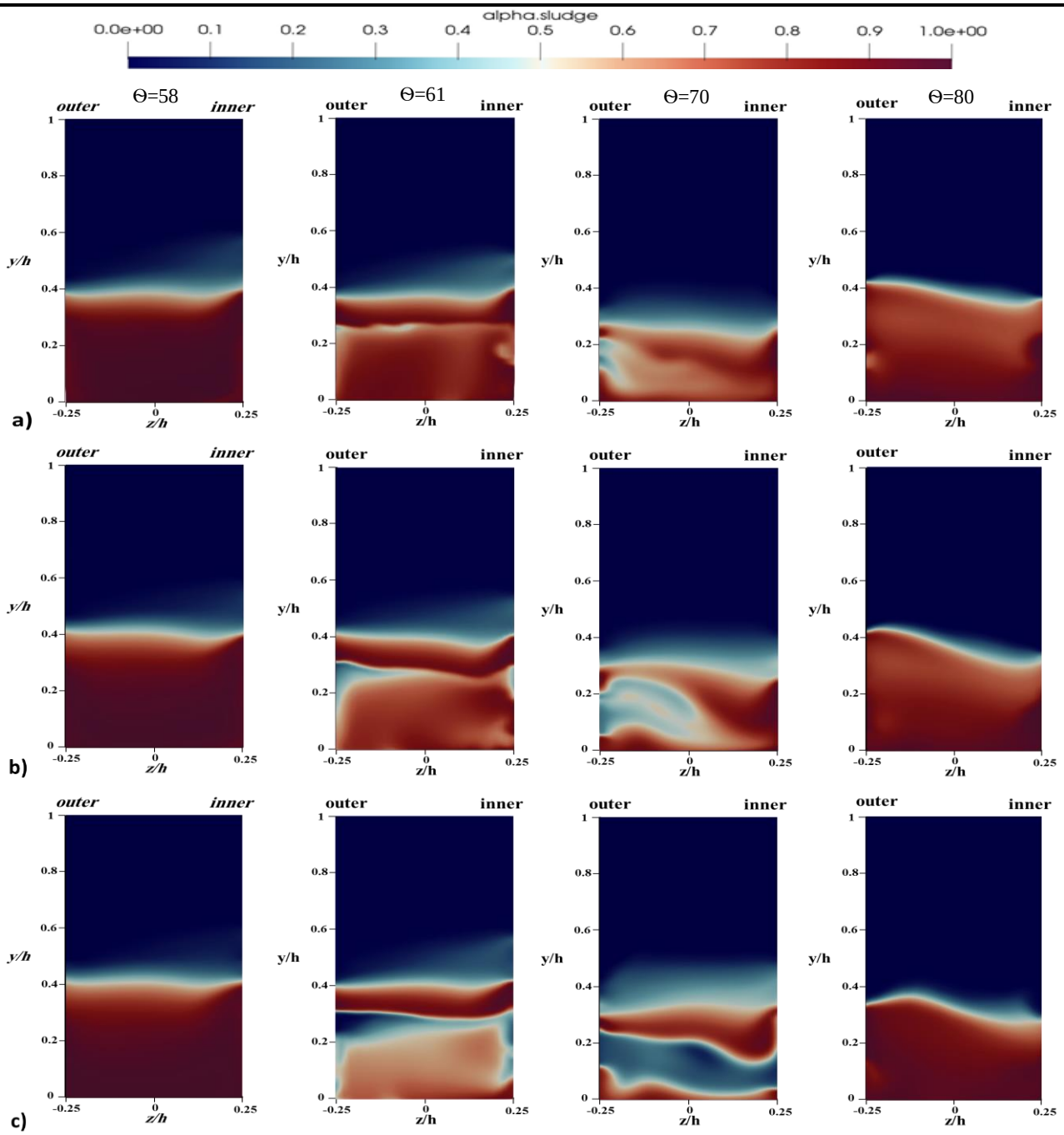


Fig. 8. The cross-sections of the concentration contours, current head at 90°, and t/t_0 =11.15 in the pre-obstacle position (58°) and post-obstacle position (61, 70, and 80°) from left to right for three models of (a) BOR, (b) BOTR, and (c) BOT.

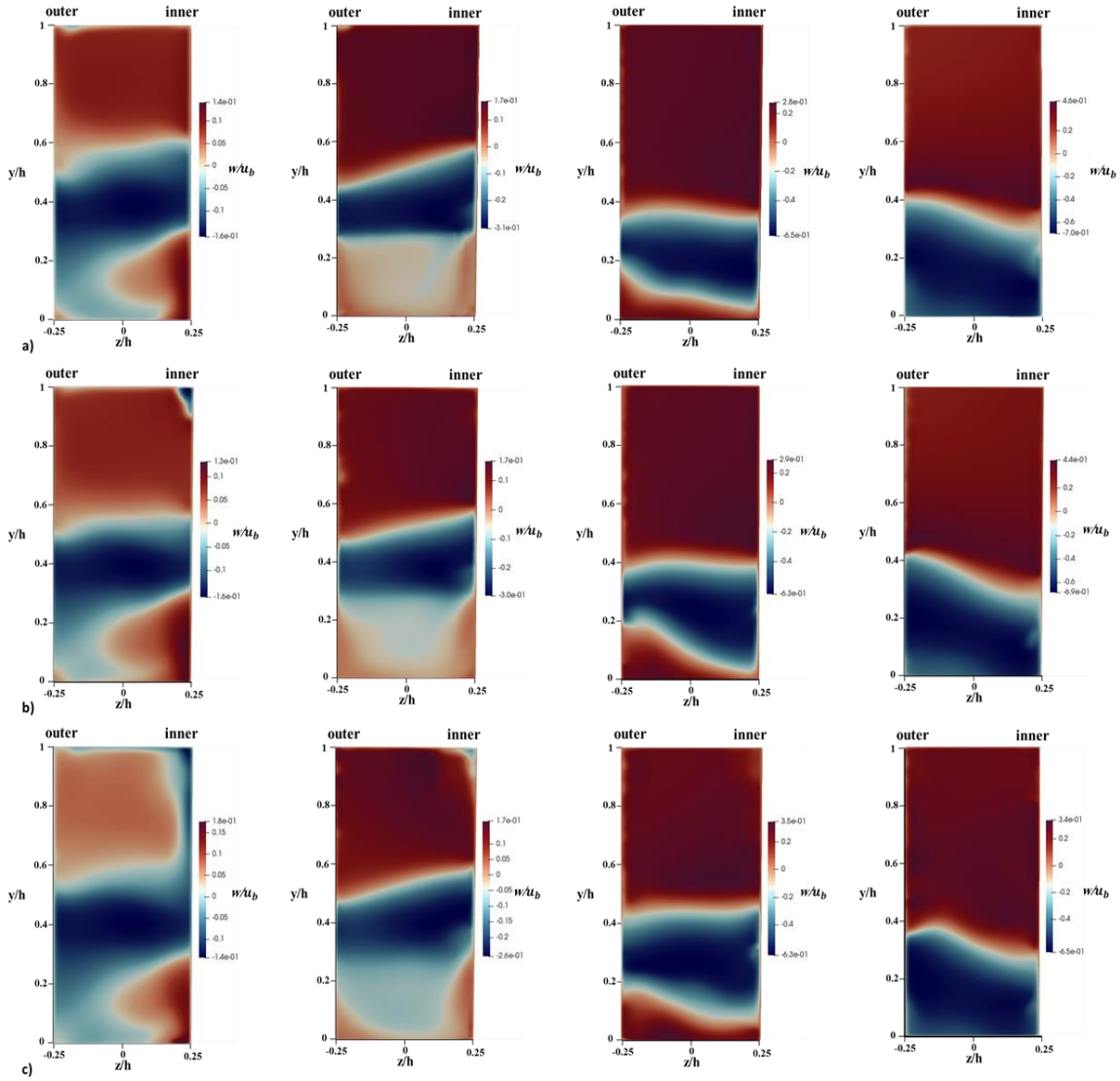


Fig. 9. The cross-sections of spanwise velocity, current head at 90° and t/t_0 =11.15 in the positions before the obstacle (58 and 50°) and after the obstacle (80 and 70°) from left to right, respectively, for the three models of (a) BOR, (b) BOTR, and (c) BOT

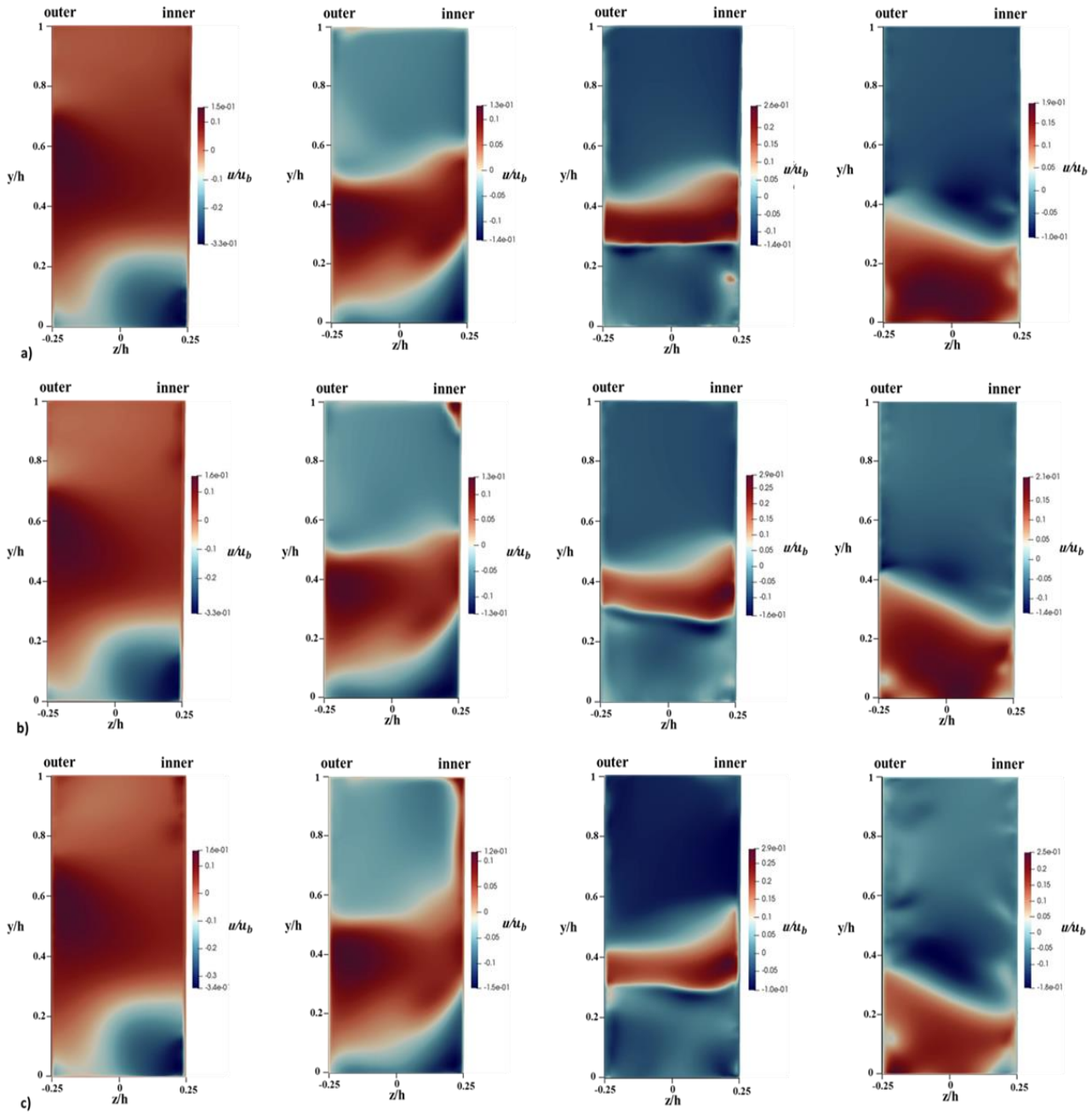


Fig. 10. The cross-sections of streamwise velocity, current head at 90° and $\frac{t}{t_0} = 11.15$ in the positions before the obstacle (35 and 50°) and after the obstacle (61 and 80°) from left to right, respectively, for the three models of (a) BOR, (b) BOTR, and (c) BOT.

However, as shown in Figure (5), in the head position, the current sections that are close to the inner bank are ahead of the sections near the outer bank and travel a shorter distance to cover a part of the curve. The streamwise velocity is irregularly distributed around the obstacle. The direction of the streamwise velocity of the current head near the bed is positive, and in terms of quantity, the BOT model has the highest value.

At the current tail, the direction of the streamwise velocity in the channel bed, in contrast to the current head, changes to negative, and like the head of the current, the streamwise velocity in the BOT model has its maximum value. Finally, it can be concluded that the triangular obstacle is less effective in reducing the streamwise velocity than the rectangular and trapezoidal obstacles. Also, the amount of streamwise velocity in the positions behind the obstacle (50 degrees) is less than that in the other positions. This may

be related to the effect of the obstacle in reducing the streamwise velocity on the positions before and near the top of the curve.

4. Conclusion

Many rivers in nature have a meandering path and may naturally be obstructed by rigid obstacles. According to previous studies, the effect of the presence of obstacles and their different shapes in the gravity-current in the curved channel has not been investigated yet. For this purpose, in the present study, obstacles in different shapes (rectangles, triangles, and trapezoids) were placed in the direction of the gravity current of lock-exchange in a channel with a curve of 120 degrees. The OpenFOAM tool was applied using the Realizable k-epsilon turbulence model. The results showed that with the gate removal and at the beginning of the formation of gravity-current, the flow would move at a constant velocity and the nose of the stream on the inner bank is ahead of the external bank. It does not mean that the streamwise velocity on the internal bank is higher. During the collision with the obstacle, the current slows down, and the nose of the current on the outer bank is overtaken by centrifugal forces on the external bank, and finally, it continues its path at a constant velocity as before the obstacle.

In an obstacle-free channel, the density in the current body decreases, and in the current head, the density of the current is higher. In the presence of an obstacle, the current behind it becomes denser. Also, the height of the dense structure of the current head in all different forms of obstacles is higher on the outer bank than on the inner bank; the difference is that in a channel with a triangular obstacle, the height of the current head dense structure is less than the other two geometries.

In the curve obstacle-free and in the head section, no secondary current occurs and most of the secondary current is in the body and tail. The presence of an obstacle reduces the amount of spanwise velocity in all places, especially behind the barrier. Thus, the amount of secondary current can be controlled using the obstacle. The direction of the secondary current at the current head is from the inner bank to the outer bank near the bed and from the outer bank to the inner bank near the interface.

The value of the streamwise velocity at the beginning of the channel is maximized on the inner bank and is maximized on the outer bank by passing through the curve vertex. In a channel with a triangular obstacle, the streamwise velocity at the current head is minimum compared to the two rectangular and trapezoidal barriers. Obstacles affect the amount of streamwise velocity, and also triangular barrier has a more negligible effect on reducing the streamwise velocity.

5. References

1. Abdollahi, A., Kabiri-Samani, A., Asghari, K., Atoof, H., & Bagheri, S. “Numerical modeling of flow field around the labyrinth side-weirs in the presence of guide vanes”. ISH Journal of Hydraulic Engineering, 23(1), 71-79 (2017).
2. Ahmed, D. I., Latrache, N., and Nsom, B. "Mixing of Saline Gravity Current Jet into Ambient Freshwater in Weakly Turbulent Regime." Journal of Hydraulic Engineering., 144(5), 05018003 (2018).
3. Amini, A., Abdollahi, A., Hariri-Ardebili, M. A., & Lall, U. “Copula-based reliability and sensitivity analysis of aging dams: Adaptive Kriging and polynomial chaos Kriging methods”. Applied Soft Computing, 109, 107524 (2021).
4. Chang, Y. S., Xu, X., Özgökmen, T. M., Chassignet, E. P., Peters, H., & Fischer, P. F. "Comparison of gravity current mixing parameterizations and calibration using a high-resolution 3D nonhydrostatic spectral element model." Ocean Modelling, 10(3-4), 342-368 (2005).
5. Cantero, M. I., Balachandar, S., García, M. H., & Ferry, J. P. "Direct numerical simulations of planar and cylindrical density currents "(2006).
6. De Falco, M. C., Ottolenghi, L., & Adduce, C. "Dynamics of gravity currents flowing up a slope and implications for entrainment." Journal of Hydraulic Engineering, 146(4), 04020011 (2020).
7. Hacker, J., P. F. Linden, and S. B. Dalziel. "Mixing in lock-release gravity currents." Dynamics of Atmospheres and Oceans 24.1-4: 183-195 (1996).
8. Hariri-Ardebili, M. A., Mahdavi, G., Abdollahi, A., & Amini, A. “An rf-pce hybrid surrogate model for sensitivity analysis of dams.” Water, 13(3), 302 (2021).
9. Härtel, C., Meiburg, E., & Necker, F. "Analysis and direct numerical simulation of the flow at a gravity-current head. Part 1. Flow topology and front speed for slip and no-slip boundaries." Journal of Fluid Mechanics, 418, 189-212 (2000).
10. He, Z., Zhao, L., Hu, P., Yu, C., & Lin, Y. T. "Hydrodynamics of Lock-exchange Turbidity Currents down a Slope Based on Direct Numerical Simulation." arXiv preprint arXiv:1610.00892 (2018).
11. Huang, S., Huang, W., & Shen, Q. "Effects of Bottom Obstacle Structure on Density-Induced Flow." In IOP Conference Series: Earth and Environmental Science (Vol. 455, No. 1, p. 012024) (2020).
12. Huang, H., Imran, J., & Pirmez, C. "Numerical model of turbidity currents with a deforming bottom boundary." Journal of Hydraulic Engineering, 131(4), 283-293 (2005).
13. Huppert, Herbert E., and John E. Simpson. "The slumping of gravity currents." Journal of Fluid Mechanics 99.4: 785-799 (1980).
14. Ikeda, S., & McEwan, I. K. (Eds.). "Flow and sediment transport in compound channels. " the experience of Japanese and UK research. CRC Press (2009).

15. Ismail, H., "Confluence of Density Currents Produced by Lock-Exchange." M.S. thesis, South Carolina Univ., SC (2017).
16. Kneller, B., and Buckee, C. "The structure and fluid mechanics of turbidity currents: a review of some recent studies and their geological implications." Sedimentology 47: 62-94 (2000).
17. Knight, D. W., & Hamed, M. E. "Boundary shear in symmetrical compound channels." Journal of Hydraulic Engineering, 110(10), 1412-1430 (1984).
18. Knight, D. W., & Demetriou, J. D. "Flood plain and main channel flow interaction." Journal of Hydraulic Engineering, 109(8), 1073-1092 (1983).
19. Lane-Serff, G. F., Beal, L. M., & Hadfield, T. D. "Gravity current flow over obstacles." Journal of Fluid Mechanics, 292, 39-53 (1995).
20. Lombardi, V., et al. "Gravity currents flowing upslope: Laboratory experiments and shallow-water simulations." Physics of Fluids 27.1: 016602 (2015).
21. Lombardi, V., Adduce, C., & La Rocca, M. "Unconfined lock-exchange gravity currents with variable lock width: laboratory experiments and shallow-water simulations." Journal of Hydraulic Research, 56(3), 399-411 (2018).
22. Magdaleno, F., & Fernández-Yuste, J. A. "Meander dynamics in a changing river corridor." Geomorphology, 130(3-4), 197-207 (2011).
23. Mahdinia, M., Firoozabadi, B., Farshchi, M., Varnamkhasti, A. G., & Afshin, H. "Large eddy simulation of Lock-Exchange flow in a curved channel." Journal of Hydraulic Engineering, 138(1), 57-70 (2012).
24. Ooi, S. K., Constantinescu, G., and Weber, L. J. "2D large-eddy simulation of lock-exchange gravity current flows at high Grashof numbers." Journal of Hydraulic Engineering, 133(9)., 1037-1047 (2007).
25. Ooi, S. K., Constantinescu, G., and Weber, L. "Numerical simulations of lock-exchange compositional gravity current." Journal of Fluid Mechanics, 635, 361 (2009).
26. Ottolenghi, L., Adduce, C., Inghilesi, R., Roman, F., & Armenio, V. "Mixing in lock-release gravity currents propagating up a slope." Physics of Fluids, 28(5), 056604 (2016).
27. Ottolenghi, L., Adduce, C., Roman, F., & la Forgia, G. "Large eddy simulations of solitons colliding with intrusions." Physics of Fluids, 32(9), 096606 (2020).
28. Ozan, A. Y., Constantinescu, G., & Hogg, A. J. "Lock-exchange gravity currents propagating in a channel containing an array of obstacles." J. Fluid Mech, 765, 544-575 (2015).
29. Özgökmen, T. M., Fischer, P. F., Duan, J., & Iliescu, T. "Three-dimensional turbulent bottom density currents from a high-order nonhydrostatic spectral element model." Journal of Physical Oceanography, 34(9), 2006-2026 (2004).
30. Paik, J., Eghbalzadeh, A., & Sotiropoulos, F. "Three-Dimensional unsteady RANS modeling of discontinuous gravity currents in rectangular domains." Journal of Hydraulic Engineering, 135(6), 505-521 (2009).
31. Rottman, J. W., Simpson, J. E., Hunt, J. C. R., & Britter, R. E. "Unsteady gravity current flows over obstacles: Some observations and analysis related to the phase II trials." Journal of Hazardous Materials, 11, 325-340 (1985).
32. Shin, J. O., S. B. Dalziel, and P. F. Linden. "Gravity currents produced by lock exchange." Journal of Fluid Mechanics 521 (2004).
33. Simpson, J. E. "Gravity Currents: In the Environment and the Laboratory, 2nd edn." Cambridge University Press (1997).
34. Steenhauer, K., Tokyay, T., & Constantinescu, G. "Dynamics and structure of planar gravity currents propagating down an inclined surface." Physics of Fluids, 29(3), 036604 (2017).
35. Sequeiros, O. E. "Estimating turbidity current conditions from channel morphology: A Froude number approach." Journal of Geophysical Research: Oceans, 117(C4) (2012).
36. Tokyay, T., & Constantinescu, G. "The effects of a submerged non-erodible triangular obstacle on bottom propagating gravity currents." Physics of fluids, 27(5), 056601 (2015).
37. Tokyay, T., Constantinescu, G., Gonzalez-Juez, E., & Meiburg, E. "Gravity currents propagating over periodic arrays of blunt obstacles: Effect of the obstacle size." Journal of fluids and structures, 27(5-6), 798-806 (2011).
38. Ungarish, M. "An introduction to gravity currents and intrusions." CRC press (2009).
39. Wormleaton, P. R., Allen, J., & Hadjipanos, P. "Discharge assessment in compound channel flow." Journal American Society of Civil Engineers, Hydraulics Division (1982).
40. Wu, C. S., & Ouyang, H. T. "Flow morphology in bottom-propagating gravity currents over immersed obstacles." AIP Advances, 10(11), 115103 (2020).
41. Yin, X., He, Y., Lu, C., Gao, S., & Liu, Q. "Experimental Study on Front Spreading of Lock-Exchange Gravity Current with Long Lock Length." Journal of Engineering Mechanics, 146(1), 04019113 (2020).
42. Zhou, J., & Venayagamoorthy, S. K. "How does three-dimensional canopy geometry affect the front propagation of a gravity current?." Physics of Fluids, 32(9), 096605 (2020).
43. Zhou, J., & Venayagamoorthy, S. K. "Numerical simulations of intrusive gravity currents interacting with a bottom-mounted obstacle in a continuously

stratified ambient." Environmental Fluid Mechanics, 17(2), 191-209 (2017).